THE ASTROPHYSICAL JOURNAL, 491:L39–L42, 1997 December 10

THE X-RAY SPECTRUM OF THE PLERIONIC SYSTEM PSR B1509−58/MSH 15−52

D. MARSDEN, P. R. BLANCO, D. E. GRUBER, W. A. HEINDL, M. R. PELLING, L. E. PETERSON, AND R. E. ROTHSCHILD
Center for Astrophysics and Space Sciences, University of California San Diego, La Jolla, CA 92093
AND
A. H. ROTS,[1] K. JAHODA, AND D. J. MACOMB[1]
Laboratory for High Energy Astrophysics, Code 660, NASA Goddard Space Flight Center, Greenbelt, MD 20771
Received 1997 August 25; accepted 1997 October 10; published 1997 November 6

ABSTRACT

We present the results of observations of the PSR B1509−58/MSH 15−52 system in X-rays (2–250 keV) by the *Rossi X-Ray Timing Explorer*. The spectra of the peak of the pulsed component (radio phase 0.17–0.53) is fitted by a power law of photon index 1.36 ± 0.01, with no evidence of a high-energy spectral break seen up to ∼200 keV. For the off-pulse spectral component, the spectrum from 2–250 keV is fitted by a power law of photon index 2.215 ± 0.005. An iron emission line at 6.7 keV with an equivalent width of 129 eV improves the fit, but only at a marginal significance. Thermal bremsstrahlung and Raymond-Smith models produce much worse fits to the unpulsed data. The lack of a high-energy spectral break in the pulsed emission implies an efficiency of ≥3% in the conversion of pulsar spin-down energy to pulsed X-rays in the system.

Subject headings: ISM: individual (MSH 15−52) — pulsar: individual (PSR B1509−58) — stars: neutron

1. INTRODUCTION

PSR B1509−58 was discovered in X-rays by the *Einstein* satellite (0.2–4 keV; Seward & Harnden 1982), and subsequent radio observations (Manchester, Tuohy, & D'Amico 1982) confirmed both the 150 ms period and the highest spin-down rate of any known pulsar of $\dot{P} \sim 1.5 \times 10^{-12}$, which implies a rotational energy loss rate of $\sim 2 \times 10^{37}$ ergs s^{-1}, assuming a neutron star moment of inertia of 10^{45} g cm^2. More recent 0.1–2.4 keV X-ray observations by the *ROSAT* satellite (Greiveldinger et al. 1995; Brazier & Becker 1997) revealed a complex morphology for the pulsar/supernova remnant system, possibly involving interactions via collimated outflows from the pulsar.

In hard X-rays, the PSR B1509−58/MSH 15−52 system was observed by *Ginga* (2–60 keV; Kawai, Okayasu, & Sekimoto 1992), and the pulsed and nonpulsed emission was modeled with power laws of photon indices 1.33 ± 0.06 and 2.15 ± 0.02, respectively. A "weak" iron line was also reported in the phase-averaged *Ginga* spectrum, at an energy of 6.7 keV. Observations at higher energies by balloon-borne instruments (94–240 keV; Gunji et al. 1994), and by the BATSE instrument aboard the *Compton Gamma-Ray Observatory* (30–800 keV; Wilson et al. 1993) have suggested a possible steepening of the pulsed spectrum, which is required for consistency with upper limits obtained at roughly MeV (Fierro 1995) and TeV (Nel et al. 1993) energies.

The nonpulsed component of the high-energy X-rays, presumably dominated by the nebular emission, has not been studied above ∼60 keV. Observations in the energy range 0.1–10.0 keV by *ASCA* (Tamura et al. 1996) have revealed a combination of thermal and nonthermal flux from the system, consistent with the picture of a compact pulsar nebula (a "plerion") surrounded by thermal emission from gas associated with the supernova remnant. The imaging spectrometers aboard *ASCA* showed that the X-ray emission at energies ≥2 keV in the region of the supernova remnant is dominated by the flux from the pulsar and compact nebula.

Recently, Rots et al. (1997) presented an X-ray timing analysis of PSR B1509−58 which confirmed the pulsed spectral shape and radio/X-ray phase lag seen by *Ginga*. In addition, the pulsed spectral index was found to be consistent with a constant value throughout the pulse, at odds with the behavior seen in hard X-rays from the Crab, another young, isolated pulsar (Ulmer et al. 1994).

2. DATA AND ANALYSIS

The plerionic system PSR B1509−58/MSH 15−52 was observed by the High Energy X-Ray Timing Experiment (HEXTE) and the Proportional Counter Array (PCA) instruments aboard the *Rossi X-Ray Timing Explorer* (*RXTE*) satellite on a number of occasions in 1996 during both the in-orbit checkout and the first observing period. The latter data consist of proprietary observations used in Rots et al. (1997). The HEXTE instrument consists of two clusters of collimated NaI/CsI phoswich detectors with a total net area of ∼1600 cm^2 and an effective energy range of ∼15–250 keV (Gruber et al. 1996). HEXTE background estimation utilizes off-source data obtained through reorientation of the detectors' viewing directions. The PCA instrument consists of five collimated xenon proportional counter detectors with a total net area of 7000 cm^2 and an effective energy range of 2–60 keV (Jahoda et al. 1996). For the PCA instrument, the instrumental background estimate is determined from modeling of both the internal background of the detectors and the background due to cosmic X-ray flux and charged particle events.

The arrival times of the photons were corrected to the solar system barycenter using the JPL DE200 ephemeris and the source coordinates R.A. (J2000) = $15^h13^m56^s.627$ and decl. (J2000) = $-59°8'9''.54$. The absolute pulse phase of each X-ray photon was then determined from the appropriate radio timing ephemeris from the ongoing monitoring campaign using the Parkes Telescope (Kaspi et al. 1994). Description of the radio observations and timing ephemerides used in the analysis are given in Rots et al. (1997). The phase ϕ at time t was obtained from the standard formula $\phi(t) = \phi(t_0) + \nu(t - t_0) + \frac{1}{2}\dot{\nu}(t - t_0)^2 + \frac{1}{6}\ddot{\nu}(t - t_0)^3$, where t_0 is the barycentric ep-

[1] Universities Space Research Association.

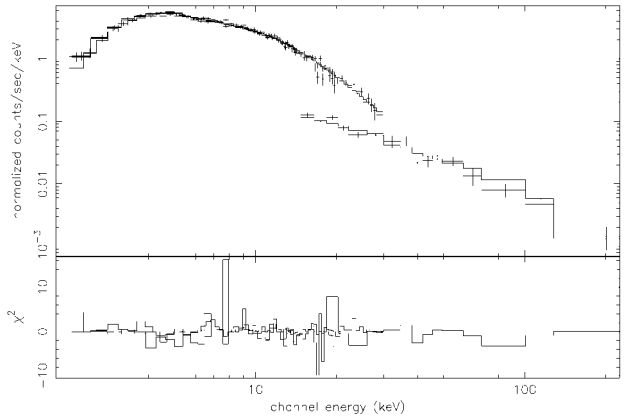

FIG. 1.—Spectral fit of the pulsed data to the model given in Table 1, showing the counts data with the fitted model overplotted as a solid line (*upper panel*) and the residuals (*lower panel*). The PCA data (2–30 keV) have been multiplied by a factor of 0.6 to account for uncertainties in the effective area calibrations of PCA and HEXTE. The HEXTE data have been co-added for clarity.

och corresponding to the radio timing ephemeris, which is defined as $t_{0\mathrm{geo}}$ rounded to two decimal places in MJD. Upon determining the absolute phase of each photon, a folded light curve was obtained for each energy channel relative to the appropriate radio ephemeris. Binning in pulse phase then produced pulsar spectra as a function of the pulse period. Discussion of the absolute timing accuracy of the instruments aboard *RXTE* is given elsewhere (Rots et al. 1997), but the total uncertainty in the absolute timing is on the order of ~10 μs, which is an insignificant (<0.1%) fraction of the PSR B1509–58 pulse phase.

3. SPECTRAL RESULTS

The pulse profile of PSR B1509–58 consists of a single asymmetrical peak below ~50 keV, which possibly develops additional components at higher energies (Rots et al. 1997). For the spectroscopic analysis, the pulsed flux was taken from photons with absolute phase 0.17–0.53, which encompasses the entire pulse peak, and the off-pulse flux used photons with phases 0.77–1.07, corresponding to regions of the light curve away from the pulse peak (Rots et al. 1997). For the PCA and HEXTE data, the off-pulse spectrum was obtained by subtracting the background model flux (PCA) or the off-source flux (HEXTE) from the off-pulse flux. The PCA background model was obtained using the program PCABACKEST, which models the time-varying detector background, in addition to the constant sky background, as a function of spacecraft position. Because the HEXTE was in the nonrocking mode for most of the observations, only ~10% of the 15–250 keV data was available for the off-pulse spectral analysis. To obtain the pulsed spectrum, the off-pulse flux was subtracted from the pulsed flux.

The PCA data and the HEXTE data were fitted simultaneously to various spectral models using XSPEC 10.0. Because of the changing detector gains in the PCA between observations, the PCA data with the same gain were combined and fitted simultaneously to the summed, gain-controlled HEXTE data from each cluster. For the pulsed spectral fits, PCA data in the energy range 2–30 keV were used, and for the off-pulse analysis, PCA data from 2–20 keV were used because of uncertainties in the background model above ~20 keV. HEXTE data in the energy range 17–250 keV were used in both spectral fits, and the data from all the observation days were added (for each cluster). In all fits, the relative normalization between the PCA and HEXTE was a free-fitted parameter to account for uncertainties in the effective open area of the two instruments. The normalization factor of the HEXTE was found to be 60% of the PCA normalization. For the off-pulse spectral fit, the PCA background model produced large residuals for much of the data in the area of the xenon L edge (4–5 keV). As a result of this, only 50% of the PCA data were used in the spectral analysis.

TABLE 1

SPECTRAL FIT RESULTS

Model Parameter	Pulsed Emission	Off-Pulse Emission	Off-Pulse Emission
Normalization[a]	6.07 ± 0.21	52.88 ± 0.43	53.55 ± 0.44
Photon index	1.358 ± 0.014	2.200 ± 0.005	2.215 ± 0.005
N_{H}[b]	1.27 ± 0.23	0 (fixed)	0 (fixed)
E_l[c]	...	...	6.71 ± 0.05
N_l[d]	...	...	1.77 ± 0.27
χ^2_ν	0.99	1.34	1.14
ν	862	763	761

[a] 10^{-3} photons cm^{-2} s^{-1} kev^{-1} at 1 keV.
[b] Neutral hydrogen absorption (10^{22} H Atoms cm^{-2}).
[c] Line centroid energy (keV).
[d] Total flux in line (10^{-4} photons cm^{-2} s^{-1}).

The pulsed spectrum from PSR B1509−58 (Fig. 1) is fitted equally well by both power-law and thermal bremsstrahlung models. We adopt the power-law model here, however, because nonthermal models are clearly favored in the extrapolation to higher energies (Wilson et al. 1993). The best-fit parameters for the power-law fit to the pulsed spectrum are given in Table 1. The fitting algorithm used by XSPEC is a modified Levenberg-Marquardt routine (Bevington 1969), and the errors for each parameter in Table 1, obtained with all the other parameters fixed at their best-fit values, are 1 σ. The unpulsed 2–250 keV spectrum was fitted to power-law, bremsstrahlung, and Raymond-Smith plasma models. The latter two models seriously underpredicted the high-energy (HEXTE) X-ray flux of the unpulsed component, and the power-law model produced the best fit to the data. The addition of a narrow Gaussian line at ~6.7 keV improved the fit, with an FTEST significance of 1%. Because of systematic uncertainties in the PCA background model at energies below ~3 keV, the intervening column density was set to zero in the unpulsed spectral fits. This had a minimal effect on the results because of the insensitivity of the PCA to small absorption columns ($N_{\mathrm{H}} < 10^{22}$ cm^{-2}). Figure 2 shows the counts spectrum of the unpulsed data, fitted to the model with the Gaussian line. The apparent absorption feature at ~5 keV is caused by imperfect modeling of xenon lines in the instrument response and background model. The best-fit parameters of the power-law and Gaussian line model and the single power-law model for the unpulsed data are given in Table 1.

4. DISCUSSION

The best-fit value of the low-energy neutral hydrogen absorption obtained in fitting the pulsed component is $N_{\mathrm{H}} = (1.27 \pm 0.23) \times 10^{22}$ cm^{-2}, which is higher than the value of $(0.59 \pm 0.06) \times 10^{22}$ cm^{-2} obtained by *ASCA* for the thermal cloud only ~8′ from the pulsar position (Tamura et al. 1996). To investigate the possible inconsistency between the pulsed N_{H} and the lower value, the best-fit contours were calculated as a function of N_{H} and the photon index using the "error" routine of XSPEC, which calculates the contours of the fit statistic as a function of two parameters while holding the other parameters fixed. The results indicate that a value as low as

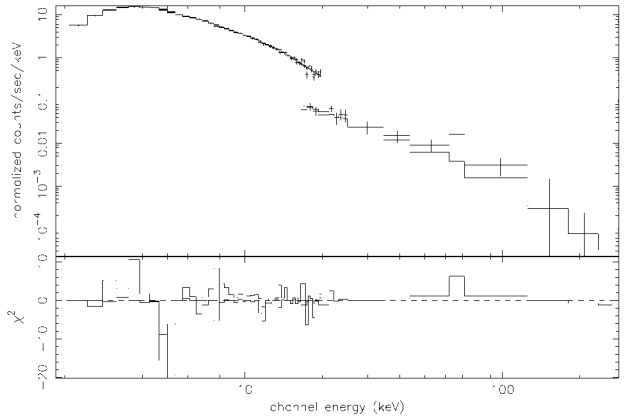

FIG. 2.—Same as Fig. 1, but with the off-pulse data. Addition of a narrow Gaussian line at 6.7 keV to the power-law model improved the fit significantly. The feature at ~5 keV is a result of oversubtraction of xenon lines in the background model.

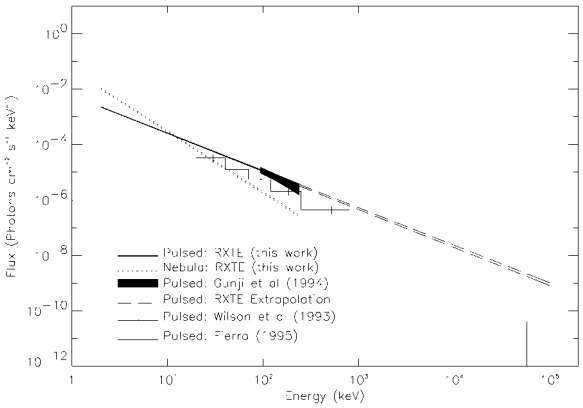

FIG. 3.—Broadband high-energy photon spectrum of PSR B1509−58/MSH 15−52. The dashed lines encompass the 1 σ error region of the extrapolated *RXTE* pulsed spectrum, and the dotted lines show the best-fit photon spectrum for the unpulsed data over the *RXTE* energy range. The extrapolated pulsed spectrum from PSR B1509−58 overpredicts the EGRET gamma-ray flux by 1–2 orders of magnitude.

$N_{\rm H} \sim 0.6 \times 10^{22}$ cm^{-2} is still allowable at the 99% confidence level. The *Ginga* values (Kawai, Okayasu, & Sekimoto 1992) for the photon index and $N_{\rm H}$ may also be consistent with the *RXTE* best fit at the 99% level. The *RXTE* value for $N_{\rm H}$ is also roughly consistent with estimations based on the radio dispersion measure of the pulsar. Assuming 10 neutral hydrogen atoms per free electron along the line of sight (Saito et al. 1997), we obtain a value of $N_{\rm H} \sim 0.8 \times 10^{22}$, given a distance of 4.2 kpc (Clark & Caswell 1977) and a dispersion measure of 253 cm^{-3} pc (Kaspi et al. 1994). We conclude that the *RXTE* does not exclude $N_{\rm H}$ values that are consistent with the interstellar absorption and pulsar dispersion measure.

The existence of a spectral break in the hard X-ray spectrum of the pulsed emission from PSR B1509−58, while not seen in the *RXTE* data, is implied by observations taken at higher energies by EGRET (Fierro 1995). Figure 3 shows the best-fit *RXTE* pulsed spectrum of PSR B1509−58 and its extrapolation to the EGRET energy range. Overplotted are the five BATSE data points (Wilson et al. 1993) from 30–800 keV and the best-fit spectrum from the 94–240 keV balloon observations of Gunji et al. (1994). Also shown is the *RXTE* unpulsed (nebular) spectrum. Aside from a factor of ~1.5 in BATSE/*RXTE* normalization, the pulsed spectrum roughly maintains its shape out to at least ~400 keV. The extrapolation to the EGRET energy range (30–100 MeV), however, exceeds the 2 σ EGRET upper limit (Fierro 1995) by a factor of 10–100, necessitating a break in the pulsed spectrum somewhere in the energy range ~0.4–30 MeV.

Because the *RXTE* pulsed photon index is less than 2, the integrated X-ray energy flux of the pulsar is actually increasing with increasing photon energy, putting constraints on the efficiencies of the processes converting the spin-down energy of the neutron star into observable radiation. If we assume that the pulsar and plerionic fluxes are due to conversion of spin-down energy with efficiencies ϵ_p and ϵ_{op}, respectively, this constraint can be expressed as

$$L_{\rm spin} \geq 4\pi d^2 \int_{E_0}^{E_b} (\eta \epsilon_p^{-1} F_p + \epsilon_{op}^{-1} F_{op}) dE, \qquad (1)$$

where $L_{\rm spin}$ and d are the pulsar spin-down luminosity ($I\Omega\dot{\Omega}$) and distance, respectively. In equation (1), F_p and F_{op} are the energy fluxes from the best-fit pulsed and unpulsed spectral models from the *RXTE* data, and η is the solid angle fraction subtended by the pulsar beam (the unpulsed plerionic emission is assumed to be isotropic). For the pulsed beaming fraction, we adopt the value $\eta = 0.3$, which is estimated from calculations by Chiang & Romani (1992). Assuming efficiencies that are independent of energy and a distance of 4.2 kpc to the pulsar and setting the lower energy $E_0 = 2$ keV and $L_{\rm spin} = 1.8 \times 10^{37}$ ergs s^{-1} yields values for the efficiencies as a function of break energy E_b given by Figure 4. The calculation in Figure 4 assumes that the entire spin-down energy budget of the pulsar is expended between the energies of E_0 and E_b. Extension of the *RXTE* pulsed and unpulsed spectra to the radio point at 1.5 GHz (Manchester, Tuohy, & D'Amico 1982) implies a total contribution to the spin-down energy budget from photons below E_0 of less than 3% of the 2–250 keV flux, given the radio flux density of 2 mJy.

The break energies in Figure 4 are relatively insensitive to the assumed spectral flattening at energies below ~2 keV because the photons at these energies carry less than 3% of the energy of the photons in the *RXTE* bandpass. Assuming a plerionic efficiency of $\epsilon_{op} = 10\%$–20% (see below), a pulsed efficiency of $\epsilon_p \geq 3\%$ is required to explain the lack of a spectral

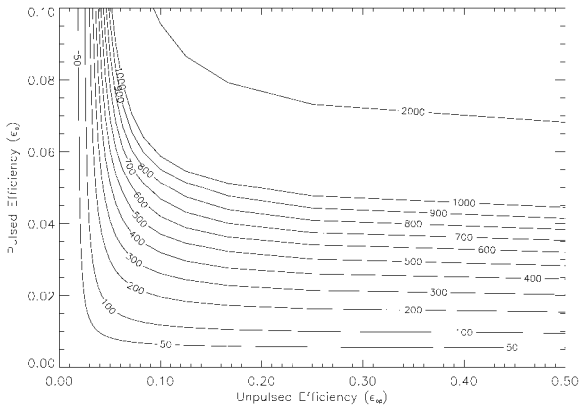

FIG. 4.—Upper break energy of the pulsed spectrum, shown as a function of the pulsed and unpulsed efficiencies. The calculation assumes a lower break energy of 2 keV and a beaming factor of 0.3 (see text). The break energies are in keV.

break below ~400 keV implied by the combined *RXTE* and BATSE observations. A plerion efficiency of $\epsilon_{op} < 10\%$ would require an even higher pulsed efficiency, but this could be eased if the pulsar has a narrow beam ($\eta < 0.3$).

The pulsed efficiency obtained above is slightly higher than the 1%–3% efficiency predicted by outer gap models of high-energy emission from young pulsars (Cheng, Ho, & Ruderman 1986). Outer gap models have difficulties explaining the lack of GeV gamma rays from PSR B1509−58 as well, because in these models the emission sites are located in the outer magnetosphere, where attenuation due to magnetic effects should be minimal (Chang, Chen, & Ho 1996). A polar cap model of the PSR B1509−58 pulsed emission (Harding, Baring, & Gonthier 1997) explains the attenuation of the gamma-ray photons in terms of magnetic photon splitting and pair production but places the spectral break at energies ≥2 MeV, which would require a relatively large pulsed efficiency of at least 7% (Fig. 4). This model also requires a polar cap for PSR B1509−58 much larger than would be produced by a simple dipole field geometry (Chang et al. 1996), indicating that perhaps a more complicated magnetic field geometry is required to explain the pulsed spectrum.

The spectral fits indicate that a power-law form is clearly favored for the unpulsed spectrum and dominates the total X-ray emission from the PSR B1509−58/MSH 15−52 system at energies ≤10 keV (Fig. 3). The *ASCA* images (Tamura et al. 1996) indicate that the ~2–10 keV emission from the system is concentrated around the pulsar rather than around the surrounding supernova remnant, implying that the unpulsed 2–250 keV emission seen by *RXTE* is caused by the pulsar plerion, not by supernova emission from MSH 15−52. The high-energy nonthermal emission from plerions is believed to be synchrotron radiation from a luminous "bubble" confined by the pressure of the surrounding supernova remnant (Rees & Gunn 1974). The internal pressure of the bubble is provided by a wind of particles and magnetic fields ejected by the pulsar. The 2–250 keV luminosity of the PSR B1509−58 plerion is $L_X = (4.7 \pm 0.9) \times 10^{35}$ ergs s^{-1}, assuming a distance of 4.2 kpc to the source.

Detailed models of the Crab Nebula (Kennel & Coroniti 1984a, 1984b) indicate that an efficiency of 10%–20% can be achieved using reasonable values for the pulsar wind speed, the plerion size, and the ratio of electromagnetic to particle energy in the wind. For the PSR B1509−58/MSH 15−52 system, Figure 4 indicates that similar plerionic efficiencies are allowed if the pulsed efficiency is not too high ($\epsilon_p \leq 3\%$). A higher pulsed efficiency would require a lower plerionic efficiency, as mentioned above. The 2–250 keV spectral index obtained for the PSR B1509−58 plerion is slightly steeper than the 17–180 keV index obtained for the Crab Nebula (Jung 1989), but the latter index show evidence for gradual steepening throughout the X-ray to gamma-ray energy range, so the two indices may be consistent.

The marginal detection of a line at ~6.7 keV suggests emission from H-like iron. The source of the iron line is most likely either the supernova remnant/plerion or the Galactic ridge. The X-ray emission from the latter was mapped out by the Japanese satellite *Tenma*, which found a mean iron line centroid of ~6.7 keV that varied in both energy and flux as a function of position (Koyama 1989). The *RXTE* line centroid is consistent with the Galactic ridge emission seen by *Tenma*, but the flux is ~3 times greater than expected from the Galactic ridge, suggesting a contribution from iron in MSH 15−52.

5. CONCLUSIONS

Observations of the PSR B1509−58/MSH 15−52 system by *RXTE* suggest that the hard X-ray spectrum from the system is dominated by nonthermal emission. The spectral shape of the pulsed and unpulsed radiation are characterized by power laws of photon index 1.358 ± 0.014 and 2.215 ± 0.005, respectively. Consideration of the *RXTE* data in the context of observations of PSR B1509−58/MSH 15−52 at other wavelengths allow us to constrain the efficiencies of the conversions of pulsar spin-down energy to observed radiation in the system. The lack of a significant spectral break in the X-ray emission out to hundreds of keV allows the efficiencies for the conversion of particle energy to X-rays in the pulsar magnetosphere and compact nebula to be constrained. The minimum pulsed efficiency is found to be 3%, assuming an efficiency for the unpulsed radiation similar to that of the Crab Nebula.

We acknowledge fruitful discussions with Richard Lingenfelter and a critical reading of the manuscript by Vicky Kaspi. The up-to-date radio timing ephemeris was provided by M. Bailes, V. Kaspi, and R. Manchester using data obtained at the Parkes radio telescope in Australia. This work was funded by NASA grant NAS5-30720.

REFERENCES

Bevington, P. R. 1969, Data Reduction and Error Analysis for the Physical Sciences (New York: McGraw-Hill)
Brazier, K. T. S., & Becker, W. 1997, MNRAS, 284, 335
Chang, H. K., Chen, K., & Ho, C. 1996, A&AS, 120, 81
Cheng, K. S., Ho, C., & Ruderman, M. 1986, ApJ, 300, 522
Chiang, J., & Romani, R. W. 1992, ApJ, 400, 629
Clark, D. H., & Caswell, J. L. 1977, MNRAS, 174, 267
Fierro, J. M. 1995, Ph.D. thesis, Stanford Univ.
Greiveldinger, C., Caucino, S., Massaglia, S., Ögelman, H., & Trussoni, E. 1995, ApJ, 454, 855
Gruber, D. E., et al. 1996, A&A, 120, 641
Gunji, S., et al. 1994, ApJ, 428, 284
Harding, A. K., Baring, M. G., & Gonthier, P. L. 1997, ApJ, 476, 246
Jahoda, K., et al. 1996, Proc. SPIE, 2808, 59
Jung, G. V. 1989, ApJ, 338, 972
Kaspi, V. M., Manchester, R. N., Siegman, B., Johnston, S., & Lyne, A. G. 1994, ApJ, 422, L83
Kawai, N., Okayasu, R., & Sekimoto, Y. 1992, in AIP Conf. Proc. 280, Proc. Workshop *Compton Observatory*, ed. M. Friedlander, N. Gehrels, & D. J. Macomb (New York: AIP), 213
Kennel, C. F., & Coroniti, F. V. 1984a, ApJ, 283, 694
———. 1984b, ApJ, 283, 710
Koyama, K. 1989, PASJ, 41, 665
Manchester, R. N., Tuohy, I. R., & D'Amico, N. 1982, ApJ, 262, L31
Nel, H. I., et al. 1993, ApJ, 418, 836
Rees, M. J., & Gunn, J. E. 1974, MNRAS, 167, 1
Rots, A. H. et al. 1997, ApJ, submitted
Saito, Y., et al. 1997, ApJ, 477, L37
Seward, F. D., & Harnden, F. R. 1982, ApJ, 256, L45
Tamura, K., Kawai, N., Yoshida, A., & Brinkmann W. 1996, PASJ, 48, L33
Ulmer, M. E., et al. 1994, ApJ, 432, 228
Wilson, R. B., et al. 1993, in Isolated Pulsars, ed. K. A. Van Riper, R. Epstein, & C. Ho (Cambridge: Cambridge Univ. Press), 257